Advanced Industrial and Engineering Polymer Research xxx (xxxx) xxx

Contents lists available at ScienceDirect

KINGFA INNOVATION CHANGE LIFE

Advanced Industrial and Engineering Polymer Research

journal homepage: http://www.keaipublishing.com/aiepr

Optimization of 3D printed polylactic acid structures with different infill patterns using Taguchi-grey relational analysis

Joel John, Deepak Devjani, Shafahat Ali, Said Abdallah, Salman Pervaiz*

Department of Mechanical and Industrial Engineering, Rochester Institute of Technology – Dubai Campus, P.O. Box 341055, Dubai, United Arab Emirates

ARTICLE INFO

Article history:
Received 23 April 2022
Received in revised form
22 June 2022
Accepted 27 June 2022

Keywords:
3D printing
FDM
PLA
Taguchi analysis
ANOVA
Grey relational analysis

ABSTRACT

In several engineering applications, the demand for robust yet lightweight materials have exponentially increased. Additive Manufacturing and 3D printing technology have the scope to make this possible at a fraction of the cost compared to traditional manufacturing techniques. Majority of the previous studies are focused mainly towards the printing parameters namely build orientation, infill density, and layer height etc. Also, most studies considered strength as an output response. However, when it comes to the cellular geometry and nozzle diameter, these parameters were found limited in the literature. Similarly, the combination of output responses such as stiffness, strength, toughness and resilience are found rarely in the previous studies. The current study is designed to capture the said gap in the literature with focus on cell geometry, nozzle diameter and strain rate by using the Taguchi design of experimentation and Grey Relational Analysis. Tensile test results performed on six different patterned samples under ASTM D638 standard suggest that square patterned samples perform the best under tension and retain more mechanical strength than the other five patterns. The grey relational analysis indicates that highest grey relational grade (GRG) was achieved for the larger nozzle diameter of 0.8 mm, strain rate of 5 mm per minute and square cellular geometry. It has been observed that highest contributing factor was nozzle diameter (48.99%), whereas cellular geometry was ranked second with (40.78%) as obtained from analysis of variance (ANOVA). The grey relational analysis simplified the complex 3D printing process optimization.

1. Introduction

The advancement in the world makes need of high-performance material at minimal cost and feasible for the same application. Researcher explored the additive manufacturing to replace them with the conventional process. Additive manufacturing is also associated with the 3D printing. 3D printing can be used in all product of automotive, biomedical and machinery. Additive Manufacturing (AM) is done by using the layer-by-layer technique. AM showed how to develop the product by using this technique, as discussed by De Leon et al. [1]. They discussed about the nano-material polymer and their behavior and strength for the AM. Wu et al. [2] discussed about the recent advancement in the field of additive manufacturing. They reviewed about the 3D printing material and techniques available. They discussed about the four different technique fused filament fabrication (FFF), Selective laser sintering (SLS), MultiJet fusion (MJF) and stereolithography (SLA).

They investigated the performance of ABS by utilizing 2 factorial and 3 factorial which include infill densities, layer thickness and raster angle. They explored the performance of 3D printed material by using the ABS by varying the different parameters under quasi static loading. Also, they varied the strain rate to check its influence on the tensile strength. Hibbert et al. [3] explored that tensile, yield and ultimate strength are affected by the infill densities. However, the layer thickness provides inconsistent properties over the time interval. The raster angle is also of the parameter which affected the modulus of toughness. They found the ultimate tensile strength (UTS) and yield strength (YS) by using the raster angle at 45 or −45° with solid fill and 10 cm/min strain rate 27.44 MPa and 23.9 MPa respectively. They strength found in the solid fill is higher than the higher fill densities due to the added density in the solid fill. They investigated the compressive loading affects under the quasi-static condition by varying the infill pattern, density and different

* Corresponding author.
E-mail address: sxpcad@rit.edu (S. Pervaiz).

https://doi.org/10.1016/j.aiepr.2022.06.002

Nomenclature

ABS	Acrylonitrile butadiene styrene
AM	Additive Manufacturing
ANOVA	Analysis of Variance
ASTM	American Society of Testing Materials
FEA	Finite Element Analysis
FDM	Fused Deposition Modeling
FFF	Fused Filament Fabrication
GRA	Grey Relational Analysis
MJF	MultiJet fusion
p	Density (g/cm^3)
PLA	Polylactic Acid
TOPSIS	Technique for Order of Preference by Similarity to Ideal Solution
UTM	Universal testing machine
UTS	Ultimate tensile strength
SEM	Scanning Electron Microscope
SLA	Stereolithography
SLS	Selective Laser Sintering
S/N	Signal to Noise Ratio
YS	Yield strength

material. Ma et al. [4] used the polylactic acid (PLA) and Mixture of PLA with carbon fiber by ratio of 70/30 respectively. In addition to this, the infill densities are 20, 40, 60 and 80% and the patterns are honeycomb, triangular and rectilinear. They follow the energy absorption principle for the 3D printed cube material for the different infill and patterns to study the characteristics of the material. From the different experimentation they found that honeycomb pattern showed the best result of energy absorption as compared with the other pattern. Furthermore, by using the more infill densities the energy absorption rate increase.

Goutham et al. [5] explored the properties of the recycled Acrylonitrile butadiene styrene (ABS) to optimize the infill rates. They used the Taguchi design to optimize the process by utilizing the S/N ratio and ANOVA analysis. Tensile and Bending test are carried out to get the responses for the different patterns and infill densities. The optimized result found at the infill density of 50% and 20% recycled ABS and enhanced the flexural strength they used 25% infill and 50% recycled ABS. Bhandari and Lopez-Anido [6] explored the polyetherimide PEI material properties by using the finite element analysis (FEA) tool and compare with the experimental result available. This model is used FEA to predict the poison ratio, shear modulus and elastic modulus and compare with the experimental values. They utilized the space frame and shell frame model to for the FEA and they found that it can predict the values with better accuracy. However, for the poison ratio they found the 20% error with the actual. They investigated the field of additive manufacturing to make an object in shorter period of time. They used the rapid prototyping machine to fabricate the product in 3 dimensional and studied its effect on the period of manufacturing. They are utilizing the ABS + hydrous magnesium silicate composite to study the effect of different testing. Christiyan et al. [7] used the ASTM standard dog bone shaped structure to study the effect of layer thickness and printing speed. From the experimentation and result they concluded that the material shows a better performance at low speed and have less layer thickness. Dawoud et al. [8] studied the ABS under both fused deposition modeling and injection modeling. They found that parameters for the Fused deposition is alter in term of raster angle to study the impact of its factor on the material properties. The result form the FDM fused deposition method showed the most prominent result in term of yield and flexural strength as compared to the injection modeling. In the experimentation they found that the impact and yield strength is maximum at the −45 or 45°. On the other hand, the flexural strength is maximum at the raster angle of 0 or 90°. Srivastava et al. [9] explored the surface methodology to using the following parameter which are raster angle, contour width, layer height and orientation for the optimization of the fusion deposition method. They found that hybrid technique is the optimal technique for this process.

Researchers [10] conducted a set of experiment to study the young modulus and tensile strength for the 3d printed part by using the fusion deposition method. They are doing a set of operation to optimize the 3d printing by fusion deposition method. This type of manufacturing is additive manufacturing and its mostly used in the biomedical field to improve it. They studied the tensile strength by altering the infill densities and number of shells. They explored the performance of ABS using the fusion deposition method in 3d printing. They are studied the anisotropy of the material to study its effect on the mechanical properties. They prepared 6 ABS based composite polymer and four blends are make and studied their effect on the properties. In addition to this, they also make the sample in the different orientation which different properties in different orientation. Torrado et al. [11] explored the tensile strength, %age elongation and perform the tensile test to study the failure. Failure is studied by using the SEM strategy by using the electron microscope and found the ways of fracturing the sample before exception.

Senatov et al. [12] explored the shape memory effect, mechanical strength and structural characteristic. They used the PLA for the 3d printing by implementing the fusion deposition method. They made the porous scaffolded structure from for the experimentation and the size of the porosity is 700 μm and the scaffolded of 30% by volume. The maximum stress recovery found at the pressure of 3.0 MPa and temperature of 30-degree C. The shape recovery SME is 98% at the last and this type of material can be used in the defect of bone replacement in the body. Fernandes et al. [13] explored the ultimate strength, yield strength, modulus of elasticity and elongation by varying the factor infill rate, raster angle, extrusion temperature and layer thickness for the PLA. Another parameter they studied is water absorption for the coating and then perform the ANOVA analysis to check the optimized condition. They used the two-protective layer for the water absorption which are acrylic and polyurethane, and the second polyurethane showed the optimized result over other. In addition to this, the other factor the strength showed an optimal value at the infill rate of 60%, thickness of layer 0.1 mm, extrusion temperature 220 °C and the raster angle of 0/90°. Lubombo and Huneault [14] investigated how mechanical performance varies regarding different infill patterns in 3D printed cellular PLA parts. Five different infill patterns were designed into dog-bone specimens and were subjected to uniaxial tensile testing and three-point bend flexural loading tests. The uniaxial tensile tests revealed that the structure with the square infill pattern showed the best mechanical properties with respect to tensile strength and tensile modulus. The hexagonal infill structure showed the best flexural properties in regard to flexural strength and modulus in both edgewise and flatwise tests. It was also observed that the hexagonal infill structure had the best stretch-dominated property over a certain range of relative densities.

Kucewicz et al. [15] modeled 3D printed cellular structures and studied the physical properties such as strength, deformation, failure, and energy absorption properties. The first geometry took the shape of a honeycomb while the second topology was a modified honeycomb structure. The third geometry had a “spiral-like” geometry. The nozzle thickness used by the 3D Printer was 0.3 mm. Each geometry was translated into a dog bone specimen

with the ASTM D638-14 Standard dimensions. It was noted that the printing directions affected certain mechanical properties. Thus, the specimens were printed in two different orientations and then analyzed. The Uniaxial Tensile tests were at a rate of 1 mm/s. The results obtained from the experiments and simulations pointed out that the size of the mesh played a role in certain parameters. The finer mesh provided lower force values. The honey-comb structures had the most energy absorption characteristic. Kucewicz et al. [16] focused on the mechanical properties of two different cellular structures manufactured by the process known as Fused Deposition Modeling (FDM). The mechanical properties of the samples were analyzed at different strain rates and the energy absorption phenomena of both topologies was studied. The two structures manufactured using a 3D Printer were honeycomb structure and a spiral geometry structure. ASTM D638-14 Standard was used for the dimension of the specimen. Uniaxial tension tests were performed using UTM at five different strain rates. It was observed that a higher strain rate caused the yield point to increase while the failure strain value decreased. The final results showed that the spiral structure is better than the honeycomb structure in terms of energy absorption. This indicates that the spiral structure can be used for applications that require a good crashworthiness. The honeycomb structure experienced brittle fracture. The spiral structure's asymmetrical geometry enabled good energy absorption characteristics under dynamic loading conditions. Kannan et al. [17] researched on how tensile properties are affected with orientation and infill density for 3D printed samples. For this study, dog bone specimens as per the ASTM D638 standard were manufactured. In this study a triple layer raster pattern was investigated. In a triple layer raster pattern, three layers were deposited at angles of 0, 90 and 45. In the vertical orientation, the number of layers is much higher when compared to a flat oriented specimen. This causes the vertical oriented specimen to have layers that are loosely bonded and fracture easily. The highest ultimate tensile strength of the specimens was found to be in the flat oriented sample with a raster pattern of 45°−90°−0°. The highest bonding was found to be in the flat oriented specimen and subsequently the flat oriented specimen had the highest Ultimate Tensile Strength.

Bodaghi et al. [18] studied the large deformations that take place in metamaterials produced by means of 3D Printing. In this work, the metamaterial structures were designed by parallelogram and hexagonal unit cells. The specimens were printed for both compressive and tensile testing. Dog bone specimens were fabricated according to the ASTM D639 Standard. The infill patterns were in hexagonal and parallelogram shapes. It was found that the metamaterial with hexagonal unit cells had a higher tensile strength in axial direction than the transverse direction. The hexagonal unit cell metamaterial also has very low compressive strength in comparison with the parallelogram unit cell metamaterial and this behavior is attributed due to its low structural density. Metamaterials were found to be anisotropic, i.e., the properties are dependent on the overall shape of the cell, loading direction and its magnitude. Moradi et al. [19] explored the effects of infill patterns on the mechanical properties of specimens manufactured by 3D Printing using PLA with fused deposition modeling (FDM). For this study, six different infill patterns were designed and printed to investigate their influence with the mechanical properties. Tensile tests were performed on these specimens. The triangular infill pattern had the highest UTS value while the grid pattern had the lowest UTS Value. The grid pattern had the lowest value for Young's Modulus, while the triangular pattern had the highest value for Young's Modulus. The wiggle infill pattern had the highest elongation percentage value and the highest energy absorbed value owing to its flexible structure. The honeycomb pattern showed the most balanced values for strength and usage of material.

Mullaveettil et al. [20] explored the influence of infill patterns on the mechanical properties of 3D Printed polymer structures. Dog bone specimens with seven different infill patterns were 3D printed. The diameter of the printing nozzle was 0.4 mm and printing was done in a flat orientation. The speed of printing was set to 20 mm/s. This ensures that the printed layers do not experience debonding. Quasi-static tensile testing and three-point flexural tests were performed on the specimens to investigate the mechanical properties such as tensile strength, flexural strength, and modulus of elasticity. The tensile test specimen was printed in line with ISO-2/1B standard and the flexural test specimen was printed with ISO 178 standard. Specimens that had cross and triangular infill patterns showed the lowest tensile strength and elongation. The influence of infill patterns was found to be more evident under tensile stress. Bending tests revealed that the cross-infill pattern performed the best. The specimen that showed the best ductility among the tested infill patterns is the PVDF-H specimen with concentric infill. Moradi et al. [21] investigated the mechanical properties of 3D printed PLA samples with a hexagonal infill. Dog bone specimen was printed in line with ISO 527-2 Standard. Tensile tests were done using a UTM. The specimens showed brittle fracture while some showed an extended plastic region before fracture. On further investigations, it was concluded that the 3D printed specimens whose layers are not fused properly will show a brittle fracture. The bond strength between the layers characterized the fracture properties. Through the tensile tests data, it was observed that the honeycomb infill pattern was an effective pattern that can be used in lightweight applications. The layer thickness was found to be directly proportional to mechanical strength of the 3D Printed honeycomb infill pattern.

Yeoh et al. [22] focused on how mechanical properties of 3D printed structures are related with regards to the infill pattern and the material. The authors in this study used PLA and cPLA to print dog bone specimens with infill patterns for tensile testing. The dog bone specimen was printed in line with ASTM D638 Standard and tensile testing was done in the specimen using a UTM at a strain rate of 5 mm/min. Stress strain curves were obtained from the tensile tests for three different infill patterns. The infill patterns used in this study were concentric, grid and zigzag patterns. It was observed that grid shaped pattern had a strong bond between the layers causing a reduced number of pores within the internal structure. The grid infill pattern with cPLA also demonstrated the highest tensile strength in comparison to the concentric and zigzag pattern. The high tensile strength of grid infill pattern is attributed because of the strong bonding and adhesion between the printed layers, hence requiring a higher amount of force to break the bond.

Khan et al. [23] focused on the effects of infill patterns on the mechanical and tensile properties in 3D printed PLA parts. Four different infill patterns were printed and studied. The dimensions of the specimens were set to be in line with ASTM D638-14 Standard. The patterns studied were rectilinear, concentric, honeycomb and Hilbert curve. The tensile tests were conducted at a strain rate of 5 mm/min and applied force of 100 kN using a UTM. The mechanical properties such as ultimate tensile strength, young's modulus and strain were investigated. The rectilinear pattern showed highest ultimate tensile strength, while the Hilbert curve pattern showed the lowest UTS value. The rectilinear and honeycomb structure underwent the highest elongation per unit length (strain) when compared to concentric and Hilbert curve infill patterns. The young' modulus was obtained from the stress strain curve by calculating the slope of the elastic region of the curve. The rectilinear pattern showed the highest young's modulus followed by concentric, honeycomb and Hilbert curve infill patterns. The rectilinear infill pattern showed the most favorable and desirable tensile mechanical properties. Akhoundi and Behravesh [24] investigated how tensile and

flexural mechanical properties are affected with respect to infill patterns in 3D printed structures. The microstructures of the specimen were analyzed and studied. For this study, four different infill patterns were investigated and tested. The patterns studied were Hilbert curve, honeycomb rectilinear and concentric infill pattern. PLA filament was used to print the specimens. The dog bone specimens for tensile testing were printed according to ASTM D638 Type IV standard. The nozzle temperature was 220 °C. UTM was utilized for performing the tensile and flexural tests. SEM was used to explore the fractured surface. It was observed that the Hilbert curve structure had the lowest ultimate tensile strength. The concentric infill pattern displayed the highest tensile modulus. In concentric and Hilbert curve pattern specimens, the number of voids observed were very low. The honeycomb pattern had a greater number of small voids in the internal structure. The voids are known to decrease the UTS of the structure. The concentric pattern also had the highest tensile strength.

Saniman et al. [25] focused on the tensile properties exhibited by different infill patterns in 3D printed structures. Six infill patterns were studied in this paper. The patterns studied were Hilbert curve, Archimedean chords, honeycomb, concentric, rectilinear, octagram spiral. The tensile test dog bone specimens were 3D printed. ASTM D638 Type III standards were applied for the dimensions of the specimens. The tensile tests were carried out on a UTM at a strain rate of 5 mm/min and a load of 5 kN. The authors reported that PLA thermoplastics have a relatively low Young's Modulus ranging from 3.4 GPa to 3.6 GPa. The rectilinear infill pattern demonstrated the highest ultimate tensile stress value (18.90 MPa) and the Hilbert curve showed the lowest UTS value. Though the mass of these infill pattern specimens were lower than that of the solid infill, the strength of these structures has been compromised. The honeycomb structures showed a low UTS value but had the highest mass. The Archimedean chords demonstrated the highest specific tensile strength. This pattern was deemed as optimal for high force applications with low mass. On the other hand, the Hilbert curve had the lowest specific tensile strength and the lowest elongation. Cabreira and Santana [26] focused on the mechanical properties exhibited by 3D printed structures with distinct infill patterns. The patterns used in this study were rectilinear, grid, triangular, and honeycomb infill patterns. Tensile tests were performed in 3D printed dog bone specimens (ASTM D638 type V specifications.) The tensile tests were done at a strain rate of 2 mm/min with a load cell of 5 kN on UTM. It was observed that the grid pattern possessed the highest elastic modulus while the honeycomb and triangular pattern had lowest elastic modulus. The rectilinear pattern had the highest UTS while the triangular pattern showed the lowest UTS. All grid patterns had the fracture region near the neck region of the dog bone specimen, while the other patterns had the fracture taking place in the middle region of the specimen. The fracture of the grid patterns near the neck region were attributed because of high stress concentrations in the neck region and low transfer of stress within the structure. The honeycomb pattern and rectilinear pattern demonstrated a high tensile strain while the grid and triangular patterns showed a relatively low tensile strain.

According to Buj-Corral et al. [27], a major factor that influences the strength of such 3D printed objects is the infill, mainly the porosity. This is a key consideration as 3D printed objects cannot be 100% solid and always have a small degree of porosity. The experiment was carried out by printing various samples with different nozzle diameters of the 3D printer, such as 0.2 mm and 0.4 mm. The infill density was also varied between 20% and 80%, while the infill pattern was set to the rectilinear grid pattern. Results show that porosity and pore size decrease with infill while samples that are printed with high infill show more irregularity in their structures. Hussin et al. [28] created 3D printed samples virtually on a Computer Aided Design (CAD) software and converted into a STL format file for a 3D printer to understand and process. These models can also be made to have infill patterns such as lines, triangles, octet, cubic, honeycomb, etc. It is important to note that to prove the validity of simulations conducted, the error percentage between the simulations and experimental results should be less than 10%. Graphs can be plotted for both simulated and experimental results for ease in comparison. The test included the 100% infill density specimen due to it being a default setting when testing simulations. This turned out to be the strongest specimen as the stress distribution was much more even compared to the other patterns. Otherwise, the Lines pattern with density of 30% produced the best results.

Chandrashekarappa et al. [29] investigated the influence of printing parameters namely layer and shell thickness, infill density, and print speed on the geometric tolerance of printed parts. The study revealed that shell thickness has dominant controlling influence on the cylindricity error of the printed part, and infill density controlled the porosity of the part. Chohan et al. [30] conducted a study towards the performance of chemical assisted vapor finishing approach to post process the FDM parts. The study used Taguchi, ANOVA and TOPSIS approaches to study the influence of orientation, finishing temperature and time involved. The study provided a major finding that temperature controls the surface finish. Higher temperature resulted in better surface finish as it controlled the fusion process more efficiently. Chohan et al. [31] in another study utilized the neural network approach to optimize the input parameters for maximum mechanical performance. Khosravani and Reinicke [32] studied the influence of raster angle and print speed on the strength of printed workpiece. The study revealed that due to the formation of voids and fusion raster pattern has greater influence on the strength as compared with the speed. Higher raster angle lowered the strength and stiffness of the workpiece material. Abdallah et al. [33] investigated the performance of multi jet fusion based 3D printed parts using grey relational analysis.

In the light of literature review, it has been identified that most commonly studied printing parameters for FDM are build orientation, layer height and printing speed. When is comes to the parameters such as cellular geometry, nozzle diameters and strain rates the material is rare to found. The study aimed to explore the combination of these parameters to bridge the gap in available literature. The study also produces results to guide users in selecting the optimum printing and testing parameters for 3D printed components. A test designed under the Predictive Taguchi Analysis and the Analysis of Variance (ANOVA) and Grey Relational. Tensile test results performed on six different patterned samples under ASTM D638 standard suggest that Square patterned samples perform the best under tension and retain more mechanical strength than the other five patterns (Table 1).

2. Experimental design and methodology

In the first stage, the research required an extensive study of the experiment goals by drawing up the literature review regarding the PLA specimen of various patterns. Using FDM technique with different nozzle diameters, various samples were scheduled to be 3D printed, and were eventually prepared to undergo mechanical testing in the form of uniaxial tension test as a single test such as this provides a lot of useful information regarding the material's behavior under tensile loading. Dog bone tensile specimens with six different infill patterns were 3D Printed using TOBECA 3D Printer. The dog-bone specimens for tensile tests were printed in line with ASTM D638 Standard. The specimens were initially designed using Autodesk Inventor 19 Cad Software, imported in STL format and then 3D printed after slicing the layer using CURA Software. The

Table 1
Summary of literature reviews.

Source	Machine/Material	Parameters	Major conclusion
Lubombo and Huneault [14]	RepRap 3D printer with PLA (1.75 mm dia and density 1.23 g/cm^3)	**Printing parameters:** • Infill density 15%, 30%, and 50% • Cellular Patterns H (Hexagonal), T (Triangular), S (Square), SD (Square-diagonal), and RSD (Reinforced Square-diagonal) **Testing parameters:** • ASTM D638-14 (tensile) type I Strain rate − 5 mm/min, 10 kN load cell • ASTM D790-10 (flexural)	Square infill pattern showed the best tensile properties. Hexagonal infill pattern outperformed others in term of flexural stiffness.
Kucewicz et al. [15]	Printer FDM 1200es SST (Stratasys Corp.) with ABSplus material.	**Printing parameters:** • Cell geometries (honeycomb, modified honeycomb and spiral) • Nozzle temp. = 300 °C • Chamber temp. = 80 °C • Layer thickness = 0.3 mm **Testing parameters:** • ASTM D638-14 standard • Topology was compressed till plastic deformation of 50% using Strain Rate − 1 mm/s	Honey-comb structures absorbed most energy. Printing direction affected properties
Kannan et al. [17]	CoLiDo X 3045 FDM Printer with ABS	**Printing parameters:** - Infill density 50−75% - Three variation of raster angles (0°−45°−90°) - Nozzle and bed temperatures 250 °C and 90 °C respectively. - Layer thickness 0.2 mm - Print speed 60 mm/s **Testing parameters:** ASTM D638 standard. Tensile Test	The highest ultimate tensile strength of the specimens was found to be in the flat oriented sample with a raster pattern of 45°−90°−0°−90°)
Kucewicz et al. [16]	1200es SST (Stratasys Corp.) with ABS-Plus	**Printing parameters:** Cuboid (40 × 40 × 20 mm) Cell wall thickness of 1.2 mm (honeycomb) and 1.35 mm (spiral) structure **Testing parameters:** ASTM D638 Standard 0.1 mm/s, 1 mm/s, 10 mm/s and 100 mm/s	Spiral like structure showed better energy absorption characteristic.
Bodaghi et al. [18]	FlashForge New Creator Pro 3D printer with PLA	**Printing parameters:** Layer height = 0.2 mm Nozzle Temp. = 185 °C Platform Temp. = 70 °C Chamber Temp. = 25 °C Printing speed = 40 mm/s **Testing parameters:** ASTM D639 Standard Tensile Test	Hexagonal pattern showed better tensile properties in axial direction. Parallelogram pattern showed high compressive strength.
Moradi et al. [19]	Sizan3N FDM 3D printer with PLA	**Printing parameters:** Nozzle Temp. = 220 °C Platform Temp. = 60 °C Printing speed = 20 mm/s Raster angle = 45 Density = 50% Layer thickness = 0.2 mm Infill Patterns = Full honeycomb, rectilinear, triangular, fast honeycomb, grid, and wiggle **Testing parameters:** ASTM D638 Standard Strain rate − 0.1 mm/min Tensile Test	Honeycomb pattern showed balanced and optimum tensile values. Wiggle pattern showed highest energy absorption.
Mullaveettil et al. [20]	Ultimaker 2+ with Polyvinylidene fluoride (PVDF)	**Printing parameters:** Patterns: linear (lines), cubic, cross, concentric, octet, zigzag and triangular Infill density 75% Nozzle dia 0.4 mm Extrusion temperature 230 °C Build plate temperature 90 °C Printing speed 20 mm/s Extrusion multiplier 1 Layer thickness 0.1 mm Build orientation Flat Raster orientation Longitudinal	Cross and triangular infill patterns demonstrated the lowest UTS and elongation.

(*continued on next page*)

Table 1 (*continued*)

Source	Machine/Material	Parameters	Major conclusion
		Shell thickness 0.8 mm **Testing parameters:** ISO-2/1B standard Printing speed − 20 mm/s Nozzle diameter − 0.4 mm	
Moradi et al. [21]	PLA	**Printing parameters:** Nozzle dia = 0.45 mm Infill Pattern = Honey comb Build Orientation = 45° Print Speed = 3600 mm/min **Testing parameters:** ISO 527-2 Standard Tensile Test	Honeycomb pattern showed characteristics that are suitable for lightweight applications. Increasing the layer thickness increased the mechanical strength.
Yeoh et al. [22]	RepRap 3D printer with PLA and cPLA materials.	**Printing parameters:** Printing temp. 200C Layer height 0.2 mm Printing speed 14 mm/s Layer thickness 0.2 mm Wall thickness 0.8 mm Infill Pattern zigzag, grid and concentric Infill Density 80% **Testing parameters:** ASTM D638 Standard Strain rate − 5 mm/min Tensile Test	Grid infill pattern had the highest UTS. Grid pattern had strong bonding and adhesion between the layers causing a higher UTS.
Khan et al. [23]	REPRAP 3D Printer with PLA	**Printing parameters:** Infill patterns of rectilinear, concentric, honeycomb and Hilbert curve **Testing parameters:** ASTM D638-14 Standard Strain rate − 5 mm/min Applied force- 100 kN Tensile Test	Rectilinear pattern had the highest UTS. Honeycomb and rectilinear pattern underwent highest elongation per unit length and the rectilinear infill pattern demonstrated the most favorable mechanical properties.
Akhoundi and Behravesh [24]	FDM with PLA	**Printing parameters:** Nozzle diameter 0.4 mm Air gap −0.05 mm Extrusion (bead) width 0.4 mm Layer height 0.2 mm Build direction XYZ Fill percentage 20, 50 and 100% Print speed 40 mm/s Infill/Perimeter Overlap 40% Infill Patterns: Concentric, rectilinear, Hilbert curve, and honeycomb patterns **Testing parameters:** ASTM D638 Type IV standard.	Concentric pattern had the highest UTS and tensile modulus. Hilbert curve showed the lowest UTS.
Saniman et al. [25]	FDM with PLA	**Printing parameters:** Infill Patterns Rectilinear, concentric, honeycomb, octagram spiral, Archimedean chords, and Hilbert curve Nozzle size 0.4 mm Layer height (mm) 0.2 Density (%) 20 Infill angle 45 Nozzle temperature 210 Bed temperature 60 **Testing parameters:** ASTM D638 Type III standard. Tensile Test at Strain rate of 5 mm/min and load of 5 kN.	Rectilinear infill pattern had the highest UTS while the Hilbert curve pattern had the lowest UTS and lowest elongation.
Cabreira and Santana [26]	Prusa i3 with PLA	**Printing parameters:** Layer thickness 0.3 mm Printing speed 20 mm/s Nozzle Dia 0.4 mm Infill Patterns Rectilinear, Grid, Honeycomb and Triangle **Testing parameters:** ASTM D638 type V specifications. Tensile Test Strain rate of 2 mm/min. Load cell of 5 kN.	Rectilinear infill pattern had the highest UTS while triangular pattern showed the lowest UTS. Fracture at neck region for grid patterns were due to high stress concentrations in the neck region.
Buj-Corral et al. [27]	Sigma extruder from BCN3D with PLA material	**Printing parameters:** Nozzle Dia 0.2−0.4 mm Infill density 20, 40, 60, and 80% Layer height 0.15 mm Printing speed 60 mm/s	Porosity and pore size decrease with infill while samples. Samples that are printed with high infill show more irregularity in their structures

Table 1 (*continued*)

Source	Machine/Material	Parameters	Major conclusion
		Printing temp. 205 °C **Testing parameters:** Zeiss Metrotom 800 X-ray tomography equipment for 3D Images	
Hussin et al. [28]	QiDi Tech 3D printer with ABS	**Printing parameters:** Layer height 0.2 mm Printing temp. 230 °C Build plate temp. 80 °C Print speed 60 mm/s Lines and Triangles patterns **Testing parameters:** ASTM D638 tested at 5 mm/min (tensile) and ASTM D695 at 1.3 mm/min (compression)	Specimen with 100% infill density showed the best results and lines pattern with density of 30% produced the next best results

Concluding remarks

- Current Study
  - In the light of literature and as per the best knowledge of authors, below combination of mixed input (printing and testing) parameters with the detailed output responses rarely exists in the literature.
  - It is worth mentioning that Nozzle dia as a parameter is less studied in the literature majority of the work is on layer height, build orientation and print speed.
  - The response data was analyzed for the optimal conditions using grey relational analysis (GRA).
  - This combination of input-out data, and GRA is very rarely found in the existing literature.
- **Printing parameters**
  - Six geometric Patterns (Hexagonal, triangular, square, Diamond, Diamond angle and Square angle
  - Nozzle Dia 0.4, 0.6 and 0.8 mm

  Testing parameter

  Strain rate 1, 5 and 10 mm/min
- **Output responses**
  - Modulus
  - UTS
  - Yield Strength
  - Toughness
  - Resilience
- **Methodology**
  - Experimentation ASTM D638 type I specimens
  - Taguchi Design of Experiments
  - Grey Relational Analysis
- **Major findings**
  - The input parameter that affected the properties the most was the nozzle diameter (48.99%), followed by geometric patterns (40.78%) and strain rate (3.2%).
  - Through this study, it is observed that the square pattern printed with a nozzle diameter of 0.8 mm and tested at a strain rate of 5 mm/min was the most optimized combination for lightweight applications.

specimens were printed in the flat orientation for this study. The 3D Printer works on the principle of fused deposition modeling, wherein the melted thermal plastic continually flows through the nozzle and prints the specimen in the desired geometry. For the tensile tests, each infill pattern was printed three times and the tensile tests were conducted on all three specimens. This was done to ensure accurate and precise results are obtained from the tests.

The material used for printing the specimens was Polylactic Acid (PLA). The six different patterns used in this study were hexagonal, square, diamond, square angle, diamond angle and triangular. Mechanical tests like tensile testing, impact test and creep test were performed on the 3D Printed specimens and the output results and data was analyzed. The input parameters used for this study were infill pattern, infill density, nozzle diameter and strain rate. From the extensive literature reviews done, it was observed that the authors of the literatures used strain rates ranging from 2 mm to 5 mm to perform the mechanical tests. The three chosen Nozzle diameters were 0.4 mm, 0.6 mm and 0.8 mm, which would subsequently print numerous batches of the CAD parts designed with six different geometric patterns. These patterns include a Solid pattern as a reference. The default settings of the 3D printer, as seen in Table 2, were noted and were to be kept constant throughout the printing procedure.

The output parameters studied experimentally were ultimate tensile strength, yield strength, modulus of resilience, modulus of elasticity and the toughness or energy absorbed. Numerical analysis was also done to validate the experimental results. The experimental and numerical results were compared to the trends seen in numerous extensive literatures. The figure below depicts the approach in which this research study was performed (Fig. 1).

Fig. 2 shows the Repetier Software in which the specimens were placed and sliced before 3D printing. The specimens were sliced using CURA within the Repetier Software Fig. 3 shows the TOBECA 3D printer used to print the specimens. Fig. 4 shows the 3D printed geometric patterns that were used for this study. A total of six geometric patterns were studied and their mechanical properties were investigated. A solid pattern was used for numerical analysis in this study.

2.1. Design of experiment

The set of experiments done in this study were modeled using the Taguchi design of experiments. For the tensile tests, the Taguchi design of experiments was used to determine the corresponding strain rate that has to be used for the different geometric pattern and the nozzle diameter. The Taguchi design used in the study consisted of an L18 Array corresponding to 3 factors and 18 runs. The Taguchi design was incorporated using the Minitab 19 Software. Table 3 shows the Taguchi design used to determine the strain rates.

To prepare, a tensile test must be conducted on a solid specimen with 100% geometric density. This acts as a reference to all the other

Table 2
Default printer settings and filament information.

Parameters	Set values
Printing parameters	
Printing temperature	210 °C
Printer bed temperature	60 °C
Printing speed	40 mm/s
Infill density	100%
Layer height	0.2 mm
Filament information	
Manufacturer	NL6002
Filament print temperature	195–230 °C
Recommended speed	30–60 mm/s
Filament length	330 m
Tolerance	±0.02 mm

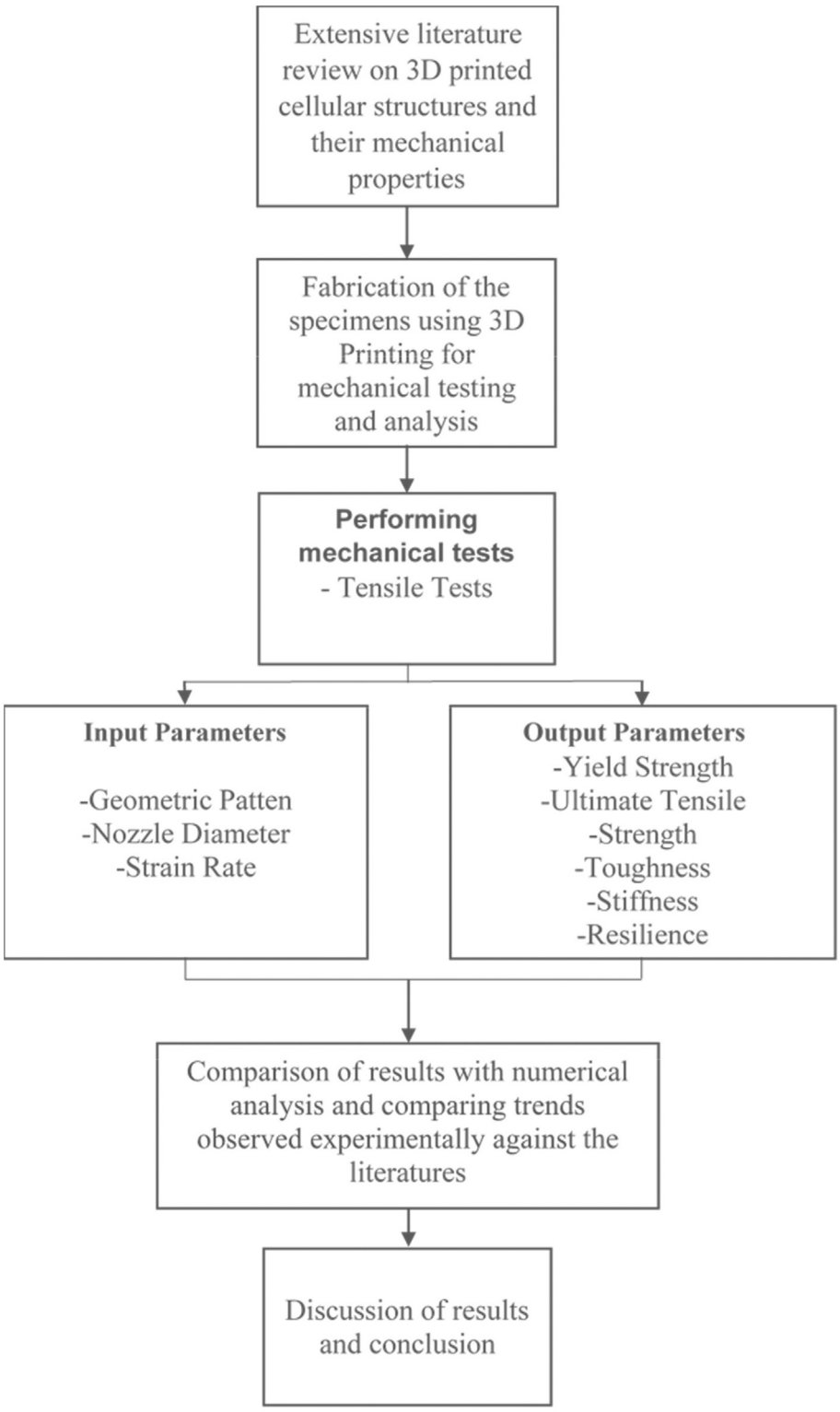

Fig. 1. Methodology of this research study.

patterned specimens that are to be tested later. Parameters that are required to be output include: Yield Strength, Tensile Strength, Young's Modulus (or Elastic Modulus), Resilience and Toughness. These five parameters were also called as the response variables. The independent variables in this study are strain rate, geometric pattern and nozzle diameter.

3. Grey relational analysis

Grey relational analysis was implemented in this study to identify the best and optimized combination of independent variables that yield the best mechanical properties. The Minitab 19 Software was used for Grey Relational Analysis. Grey Relational

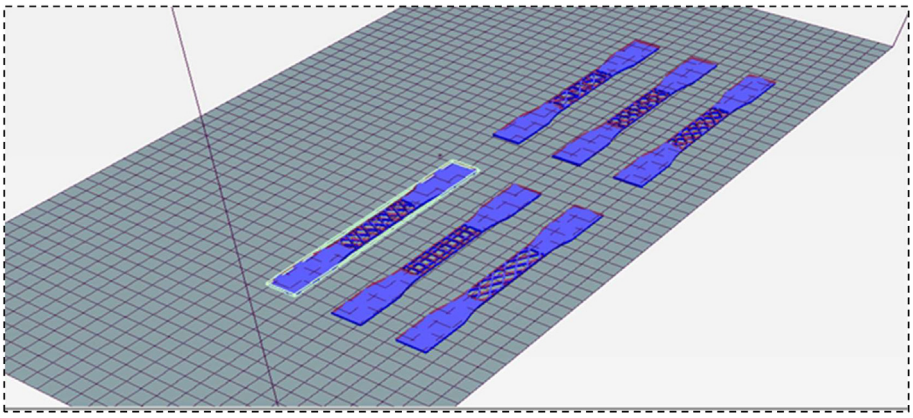

Fig. 2. Specimens placed on Repetier Software before slicing.

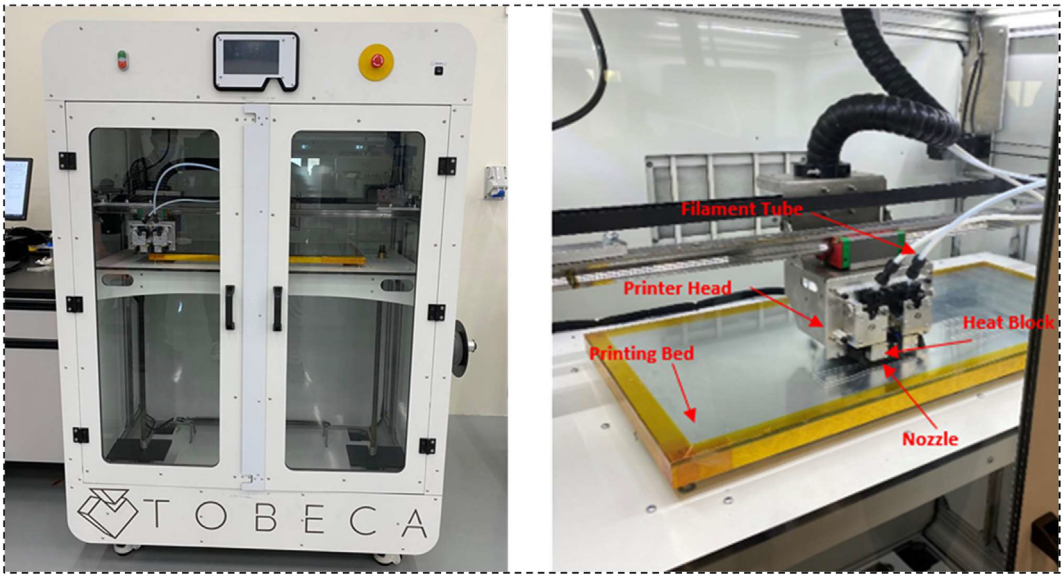

Fig. 3. TOBECA 3D printer used to fabricate the 3D Printed specimens. Sliced models of the tensile specimens designed in AUTOCAD.

Analysis was done through a multiple step sequence as depicted below in Fig. 5.

3.1. Phase 1 — Data processing

The Uniaxial Tensile tests were done on the specimens and the output data was compiled and calculations were done to process the 5 output parameters, namely, Yield Strength, Tensile Strength, Young's Modulus (or Elastic Modulus), Resilience and Toughness. The output data was processed in Minitab. After data processing, the Signal to Noise Ratio (S/N) was calculated. The S/N Ratio Tab displays three choices: smaller, nominal and larger is better. From literatures, it was seen that higher value of response variables was better in terms of mechanical properties. Thus, the larger is better option was considered to obtain the S/N Ratio values. Response Tables and Plots for Larger is better option were obtained as the response parameter. Table 4 shows the Taguchi L18 Orthogonal array output data.

3.2. Phase 2 — Normalization of data

The next phase in Grey Relational Analysis is Data Normalization. Raw data can be normalized through a sequence of steps in the Minitab 19 Software. Three options are presented to choose from for normalizing the data. They are, nominal, smaller and larger is better. For this study, the larger is better choice was selected as all the mechanical properties studied were to be of the highest value for optimized and improved performance.

For the larger is better option, a specific formula was used to normalize the data.

$$x_{ij} = \frac{y_{ij} - \max\left(y_{ij}\right)}{\max\left(y_{ij}\right) - \min\left(y_{ij}\right)} \quad (1)$$

In the above formula, y_{ij} represents the corresponding S/N Ratio data points while x_{ij} represents the resulting normalized data. The S/N Ratio data for the five studied parameters were normalized using equation (1) and Table 6 displays the obtained results (Table 5).

3.3. Phase 3 — Determining the deviation sequence

The deviation sequence of the normalized data is obtained by normalizing the data points between the values of 0 and 1. The deviation sequence is calculated using equation (2) as depicted below.

Fig. 4. Patterns used in this study printed at 0.6 mm diameter nozzle as per Taguchi DoE, (A) Patterns before testing (B) Fractured specimens after performing tensile tests (C) Shows the square angle pattern before fracture, (D) Shows the hexagonal pattern after initial fracture took place.

Table 3
Taguchi design for determining the strain rates.

Geometric pattern	Strain rate (mm/min)	Nozzle diameter (mm)
Hexagonal	1	0.8
Hexagonal	2	0.6
Hexagonal	5	0.4
Triangular	1	0.8
Triangular	2	0.6
Triangular	5	0.4
Square	1	0.6
Square	2	0.4
Square	5	0.8
Diamond	1	0.4
Diamond	2	0.8
Diamond	5	0.6
Diamond Angle	1	0.6
Diamond Angle	2	0.4
Diamond Angle	5	0.8
Square Angle	1	0.4
Square Angle	2	0.8
Square Angle	5	0.6

$$\Delta 0i\ (k) = x0\ (k) - xi\ (k) \tag{2}$$

where $\Delta 0i(k)$ represents deviation, $x0(k)$ represents reference and $xi(k)$ represents comparability. In this formula, the reference value was 1 while $xi(k)$ was the set of normalized data points. The obtained deviation sequence responses are recorded in Table 7.

The maximum deviation from the reference is 1 while the minimum deviation from the reference is 0.

3.4. Phase 4 – Determining the Grey Relational Coefficient

The Grey Relational Coefficient is calculated using equation (3). The formula includes the data points from the deviation sequence responses.

$$\varepsilon_i(k) = \frac{\Delta\min + (\psi * \Delta\max)}{\Delta ij\ + (\psi * \Delta\max)} \tag{3}$$

Fig. 5. Multistep sequence used for Grey Relational Analysis.

Table 4
Output data array.

No.	Pattern type	Strain rate (mm/min)	Nozzle diameter (mm)	Young's Modulus (GPa)	Ultimate tensile strength (MPa)	Yield strength (MPa)	Toughness (MPa)	Resilience (MPa)
1	HEX	1	0.8	0.55	10.49666667	10.10333333	27.38288403	6.002474522
2	HEX	2	0.6	0.466667	7.13	6.726666667	12.18230199	4.705910262
3	HEX	5	0.4	0.33	6	6.192666667	20.04600667	2.247234434
4	TRI	1	0.8	0.606667	12	11.87666667	22.53270906	8.116902226
5	TRI	2	0.6	0.516667	8.913666667	8.343333333	14.39097519	6.131052586
6	TRI	5	0.4	0.47	9.666666667	8.86	13.12339333	4.898373333
7	SQU	1	0.6	0.623333	10.15066667	10.04	17.59798241	7.14934609
8	SQU	2	0.4	0.496667	9	8.47	4.516733333	3.41766
9	SQU	5	0.8	0.733333	16	15.58	22.90650515	12.55874675
10	DIA	1	0.4	0.323333	6.666666667	6.139333333	10.99164333	2.74127
11	DIA	2	0.8	0.56	11.33333333	10.02666667	51.78773156	5.563851558
12	DIA	5	0.6	0.473333	8.333333333	7.176666667	33.8133677	4.264358754
13	DIAA	1	0.6	0.27	6.585333333	6.393	7.316174433	2.373344426
14	DIAA	2	0.4	0.283333	5	4.996	6.80651	1.106143333
15	DIAA	5	0.8	0.5	9.666666667	9.1	21.21705707	4.859646115
16	SQUA	1	0.4	0.313333	5.666666667	5.338	2.295363333	1.137763333
17	SQUA	2	0.8	0.493333	10.66666667	9.95	35.35137685	5.3744864
18	SQUA	5	0.6	0.413333	7	6.593333333	37.09985302	4.322621186

Δmin is the minimum value of the deviation sequence response while *Δ*max represents the maximum value of the deviation sequence response. Δij represents the corresponding data points from the deviation sequence responses. For this study, the distinguishing coefficient ψ was set to be 0.5. *Δmin* is 0 while *Δmax* is 1. Table 8 displays the Grey Relational Coefficient (GRC) of the 5 output parameters.

3.5. Phase 5 – Determining the Grey Relational Grade

The next step is to determine the Grey Relational Grade (GRG). The GRG of each experiment is determined by computing the average of the response variables from the Grey Relational Coefficient Responses. Equation (4) shows the formula used to compute the Grey Relational Grade.

$$\gamma_i \frac{1}{n}\sum_{i=1}^{n}(k) \tag{4}$$

The variable n in the equation represents the number of response variables. In this study, there were 5 response variables being studied and thus $n = 5$. The grey relational grades were then ranked and analyzed. Table 9 displays the Grey Relational Grades along with their ranks.

From Table 9 it is observed that Experiment 9 showed the highest Grey Relational Coefficients. The input variable combinations in Experiment 9 displayed the most optimum conditions. The input variable combinations used in experiment 9 were square geometric pattern printed with a nozzle diameter of 0.8 and tested under a strain rate of 5 mm/min. The means of Grey Relational Grades were also computed using the Minitab 19 Software and Table 9 displays the computed results.

Observations from Table 10 is useful to indicate the optimum values of the input variables to achieve the best mechanical properties. Level 3 for patterns, level 3 for strain rate and level 3 for nozzle diameter gives the most optimum results in regard to mechanical properties. Figs. 6 and 7 show the main effect plots for means and SN ratios.

Table 5
Signal to Noise Ratio (S/N) of output parameters.

No	S/N Ratio of Yield	S/N Ratio of Modulus	S/N Ratio of UTS	S/N Ratio of Toughness	S/N Ratio of Resilience
1	20.08929363	−5.19274621	20.42102812	20.42102812	15.56660651
2	16.55599814	−6.619864381	17.0617906	17.0617906	13.45287282
3	15.83755408	−9.629721202	15.56302501	15.56302501	7.032967616
4	21.49389135	−4.340997335	21.58362492	21.58362492	18.18780629
5	18.4267919	−5.735791131	19.00112779	19.00112779	15.75070082
6	18.94867444	−6.558042841	19.70553486	19.70553486	13.80103764
7	20.03467426	−4.105592964	20.12989133	20.12989133	17.08532642
8	18.55766821	−6.078699726	19.08485019	19.08485019	10.67457711
9	23.85134907	−2.693971478	24.08239965	24.08239965	21.97892606
10	15.76242428	−9.806990409	16.47817482	16.47817482	8.759036265
11	20.02313154	−5.03623946	21.08715325	21.08715325	14.90751069
12	17.1184555	−6.496658207	18.41637508	18.41637508	12.59707468
13	16.11409409	−11.37272472	16.37155526	16.37155526	7.507215376
14	13.97244859	−10.95404658	13.97940009	13.97940009	0.876228124
15	19.18082785	−6.020599913	19.70553486	19.70553486	13.73209289
16	14.54757139	−10.07986802	15.06655333	15.06655333	1.121038673
17	19.95646161	−6.137190786	20.56057447	20.56057447	14.60673936
18	16.38210065	−7.673991391	16.9019608	16.9019608	12.71494355

Table 6
Normalized data responses.

Sr. No	Yield strength	UTS	Modulus	Toughness	Resilience
1	0.619182778	0.637596	0.712081371	0.637595596	0.696137452
2	0.261521974	0.305097	0.547643216	0.30509657	0.595973308
3	0.188796869	0.156748	0.200835704	0.156747995	0.291751297
4	0.761364362	0.75267	0.810223219	0.752670015	0.820349048
5	0.450894643	0.497053	0.649509605	0.497053144	0.704861186
6	0.503722642	0.566776	0.554766537	0.566775712	0.612471901
7	0.613653886	0.608779	0.837347434	0.60877873	0.768105498
8	0.464142708	0.50534	0.609998331	0.50534003	0.46431736
9	1	1	1	1	1
10	0.181191792	0.24733	0.18041005	0.247329985	0.37354504
11	0.612485465	0.703529	0.730114693	0.703528998	0.664904678
12	0.318457192	0.439174	0.561839515	0.439174026	0.55541934
13	0.216789864	0.236777	0	0.236776727	0.314224621
14	0	0	0.048241738	0	0
15	0.527222566	0.566776	0.616692819	0.566775712	0.609204795
16	0.058217288	0.107607	0.148968021	0.107606977	0.011600912
17	0.605736745	0.651408	0.603258762	0.651407965	0.650651935
18	0.243919054	0.289277	0.426182566	0.289276536	0.561004828

Table 7
Deviation sequence responses.

	Yield strength	UTS	Modulus	Toughness	Resilience
1	0.380817222	0.362404404	0.287918629	0.362404404	0.303863
2	0.738478026	0.69490343	0.452356784	0.69490343	0.404027
3	0.811203131	0.843252005	0.799164296	0.843252005	0.708249
4	0.238635638	0.247329985	0.189776781	0.247329985	0.179651
5	0.549105357	0.502946856	0.350490395	0.502946856	0.295139
6	0.496277358	0.433224288	0.445233463	0.433224288	0.387528
7	0.386346114	0.39122127	0.162652566	0.39122127	0.231895
8	0.535857292	0.49465997	0.390001669	0.49465997	0.535683
9	0	0	0	0	0
10	0.818808208	0.752670015	0.81958995	0.752670015	0.626455
11	0.387514535	0.296471002	0.269885307	0.296471002	0.335095
12	0.681542808	0.560825974	0.438160485	0.560825974	0.444581
13	0.783210136	0.763223273	1	0.763223273	0.685775
14	1	1	0.951758262	1	1
15	0.472777434	0.433224288	0.383307181	0.433224288	0.390795
16	0.941782712	0.892393023	0.851031979	0.892393023	0.988399
17	0.394263255	0.348592035	0.396741238	0.348592035	0.349348
18	0.756080946	0.710723464	0.573817434	0.710723464	0.438995

Table 8
Grey Relational Coefficient.

No	Yield strength	UTS	Modulus	Toughness	Resilience
1	0.567654659	0.579774	0.634583295	0.579774405	0.621996884
2	0.403721333	0.418444	0.525013323	0.418443857	0.553081015
3	0.381329169	0.372231	0.384862793	0.372230972	0.413822087
4	0.676923742	0.669048	0.724872181	0.669048493	0.735671743
5	0.476596556	0.498531	0.587896116	0.498530901	0.62882102
6	0.501868276	0.535777	0.528969846	0.535776883	0.563362445
7	0.564113716	0.561028	0.754543218	0.561027903	0.683158568
8	0.482691973	0.502684	0.561796699	0.502684349	0.482773371
9	1	1	1	1	1
10	0.379130185	0.399147	0.378905584	0.399147416	0.443870388
11	0.563371055	0.627769	0.649447386	0.627769245	0.598734045
12	0.423175527	0.471331	0.532957855	0.471330842	0.52933542
13	0.389647795	0.395813	0.333333333	0.395812847	0.421665021
14	0.333333333	0.333333	0.344409957	0.333333333	0.333333333
15	0.513992186	0.535777	0.566054495	0.535776883	0.561296241
16	0.346792895	0.359094	0.370087465	0.359094014	0.335931407
17	0.559119473	0.589211	0.557574447	0.589211281	0.588686806
18	0.398063518	0.412976	0.465628499	0.41297622	0.532484101

Table 9
Grey Relational Grades and Rank.

No	Grade	Rank
1	0.59675673	5
2	0.463740677	12
3	0.384895199	16
4	0.69511293	2
5	0.538075099	8
6	0.533150867	9
7	0.624774261	3
8	0.506526148	10
9	1	1
10	0.400040198	14
11	0.613418195	4
12	0.485626097	11
13	0.387254369	15
14	0.335548658	18
15	0.542579338	7
16	0.354199959	17
17	0.576760658	6
18	0.444425712	13

Table 10
Means of Grey Relational Grades.

Level	Patterns	Strain rate	Nozzle diameter
1	0.4818	0.5097	0.4191
2	0.5888	0.5057	0.4906
3	0.7104	0.5651	0.6708
4	0.4997		
5	0.4218		
6	0.4585		
Delta	0.2886	0.0594	0.2517
Rank	1	3	2

3.6. Analyzing the effects of input parameters

The input parameters for this study were strain rate, nozzle diameter and geometric patterns. Tensile tests were performed on the dog bone specimens at different strain rates based on the Taguchi design. Data were processed and analyzed through Minitab Software. Taguchi Analysis was done on the Minitab Software to determine how the input parameters affect the output parameters. Table 9 obtained through the Taguchi Analysis point out that the geometric patterns highly affect the mechanical properties. The nozzle diameter used while printing was found to affect the mechanical properties lower than the geometric patterns but significantly higher than the strain rates. The mechanical properties were least affected by the strain rates at which the tensile tests were done.

3.7. Prediction of optimum values through Minitab

Through the Minitab 19 Software, the Grey Relational Grades for each experiment can be predicted. Higher the Grey Relational Grade, better is the performance. Experimental Results revealed that the square geometric pattern printed with a nozzle diameter of 0.8 mm at a strain rate of 5 mm/min gives the most optimized results. This result was further validated by predicting the Grey Relational Grades using Minitab 19.

Equation (5) is used to predict the optimum values.

$$\widehat{Y}_0 = Y_{0m} + \sum_{i=1}^{k} (Y_{0i}^{-} - Y_{0m}) \tag{5}$$

In the above equation, $\widehat{Y}_0$ stands for predicted grey relational grade, Y_{0m} stands for the total grey relational grade while Y_{0i}^{-} represents the average value.

The predicted values were generated from Minitab 19 after the input parameter values were entered. The input controllable parameters were Patterns (P), Strain Rate (S) and Nozzle Diameter (D). Table 11 shows the predicted Grey Relational grade in comparison with the experimental Grey Relational Grade along with the predicted optimum combination. The predicted optimum combination was P3S3D3, which stands for Pattern 3, Strain Rate 3 and Nozzle Diameter 3, i.e., geometric pattern of square, printed with a nozzle diameter of 0.8 mm and tested at a strain rate of 5 mm/min.

3.8. ANOVA – Analysis of variance

The variance was analyzed through Minitab to determine how each input parameter contribute towards the mechanical properties. Table 12 represents the variance table which shows the contribution percentage of each input parameter towards the mechanical properties. From the Variance Table it is observed that the Nozzle diameter contributed the most (48.99%) followed by the geometric patterns (40.78%). The mechanical properties were highly affected by the nozzle diameter by which the specimens were printed and the infill patterns. The strain rates at which the specimens were tested had the least contribution (3.21%) towards the mechanical properties.

The test results of the eighteen specimens are summarized in Table below. The Young's Modulus, Ultimate Tensile Strength, Yield

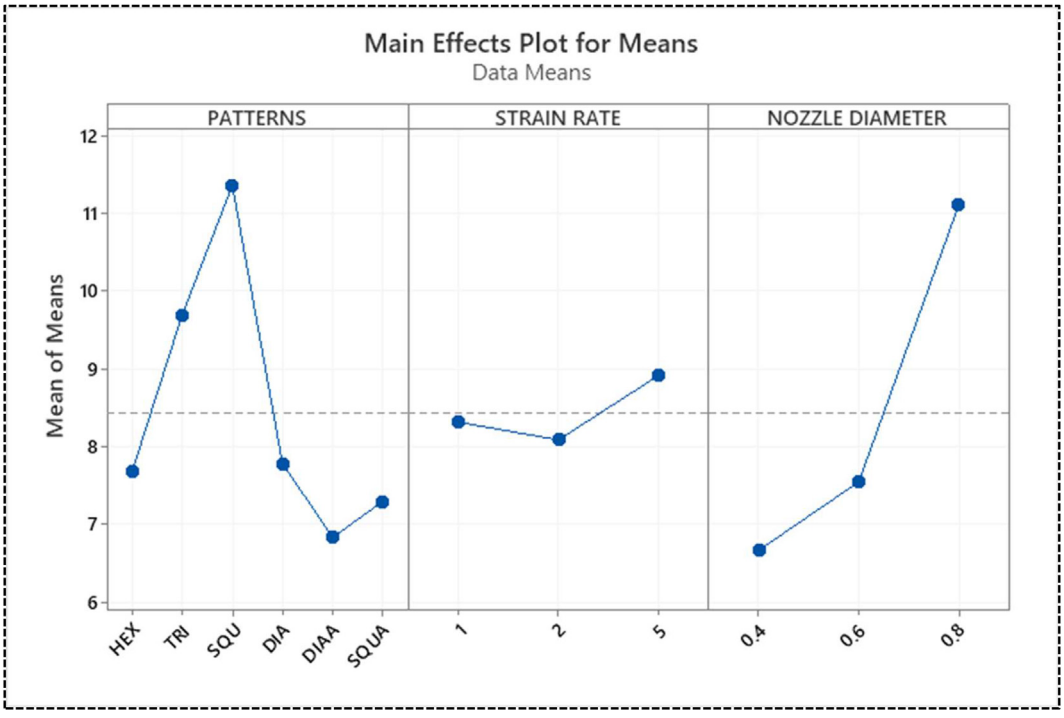

Fig. 6. Main effects plot for means.

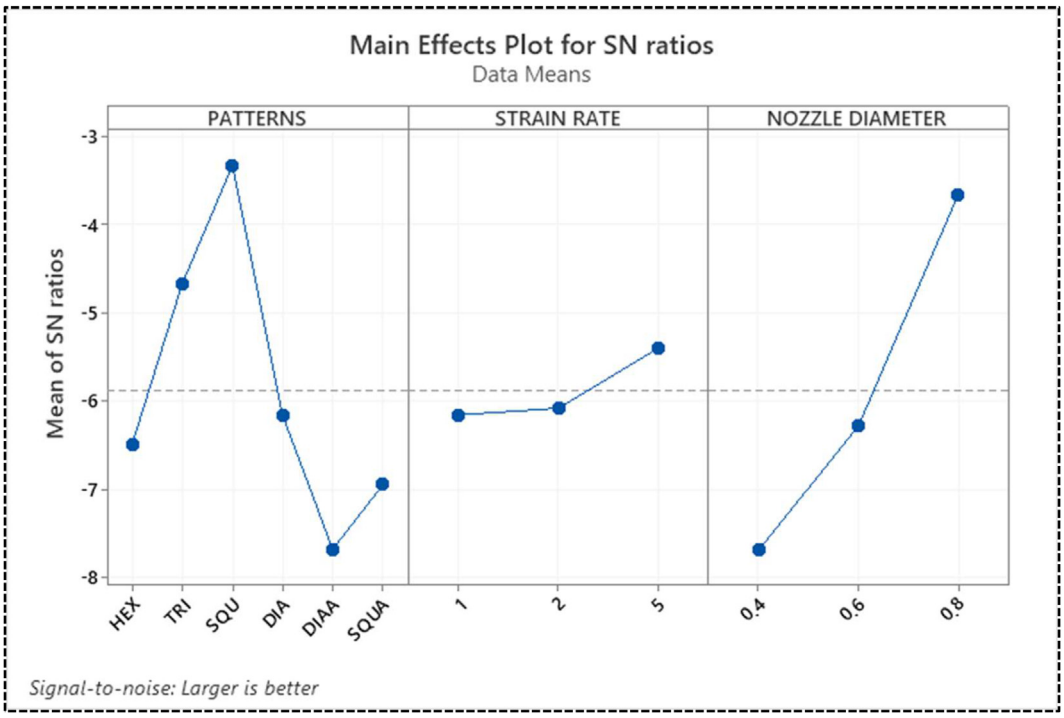

Fig. 7. Main effects plot for S/N ratios.

Table 11
Predicted Grey Relational Grade by Minitab.

	Levels	Yield stress (MPa)	UTS (MPa)	Young modulus (GPa)	Resilience (MPa)	Toughness (MPa)	Grey Relational Grade
Initial controllable parameters		15.5800	16	0.733333	12.5587	22.9065	1
Prediction		P3S3D3					0.892664
Experimentation		15.5800	16	0.733333	12.5587	22.9065	1

Table 12
Variance table.

Source	DF	Seq SS	Contribution	Adj SS	Adj MS	F-Value	P-Value
Patterns	5	0.16806	40.78%	0.16806	0.033611	9.30	0.003
Strain rate	2	0.01324	3.21%	0.01324	0.006620	1.83	0.221
Nozzle diameter	2	0.20185	48.99%	0.20185	0.100927	27.92	0.000
Error	8	0.02892	7.02%	0.02892	0.003615		
Total	17	0.41207	100.00%				

Table 13
Input reponses and their corresponding output responses.

Patterns	Strain rate	Nozzle diameter	Modulus	UTS[a]	Yield strength	Toughness	Resilience
HEX	1.000	0.800	0.550	10.497	10.103	27.383	6.002
HEX	2.000	0.600	0.467	7.130	6.727	12.182	4.706
HEX	5.000	0.400	0.330	6.000	5.975	20.046	2.247
TRI	1.000	0.800	0.607	12.000	11.877	22.533	8.117
TRI	2.000	0.600	0.517	8.914	8.343	14.391	6.131
TRI	5.000	0.400	0.470	9.667	8.860	13.123	4.898
SQU	1.000	0.600	0.623	10.151	10.040	17.598	7.149
SQU	2.000	0.400	0.497	9.000	8.470	4.517	3.418
SQU	5.000	0.800	0.733	16.000	15.580	22.907	12.559
DIA	1.000	0.400	0.323	6.667	6.139	10.992	2.741
DIA	2.000	0.800	0.560	11.333	10.027	51.788	5.564
DIA	5.000	0.600	0.473	8.333	7.177	33.813	4.264
DIAA	1.000	0.600	0.270	6.585	6.393	7.316	2.373
DIAA	2.000	0.400	0.283	5.000	4.996	6.807	1.106
DIAA	5.000	0.800	0.500	9.667	9.100	21.217	4.860
SQUA	1.000	0.400	0.313	5.667	5.338	2.295	1.138
SQUA	2.000	0.800	0.493	10.667	9.950	35.351	5.374
SQUA	5.000	0.600	0.413	7.000	6.593	37.100	4.323

[a] UTS: Ultimate Tensile Strength.

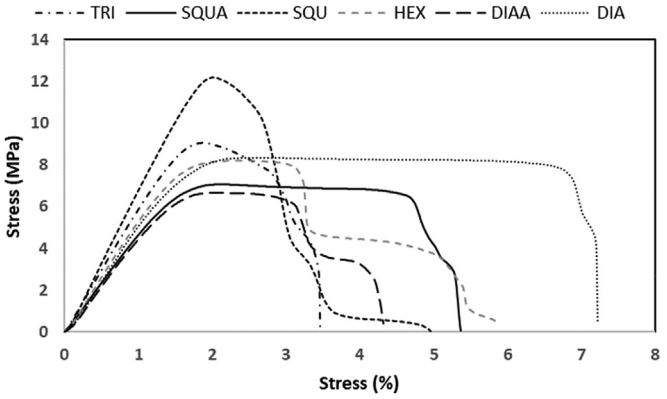

Fig. 8. Stress–strain curves obtained from experimental data.

Strength, Toughness and Resilience were some parameters whose average values were obtained from experimental data on samples that were created using ASTM standard (Table 13; Fig. 8).

In general, the trend shows that the specimen with Square pattern retains the best tensile properties and energy absorption capabilities while the Diamond Angle pattern specimen performed the worst. Another surprising trend was noticed with the Nozzle Diameters where specimens printed with a larger nozzle proved to be stronger and have better tensile properties. Therefore, the Square pattern specimen printed using the nozzle with 0.8 mm diameter displayed the best properties amongst all the eighteen tested samples with ultimate strength of 16 MPa while the Diamond Angle pattern printed using nozzle of 0.4 mm diameter was the weakest with ultimate strength of only 5 MPa. It was observed that the square geometric patterns fractured at the neck region. This behavior was noted by Cabreira and Santana [26] in grid patterns. They attributed this behavior to be present because of high stress concentration that take place near the neck region for these structures.

To further analyze the data using the Taguchi Model, the Grey Relational Coefficient of the output parameters were calculated and each of the eighteen specimens were ranked using a Grade assigned to each specimen from best to worst in order of tensile properties (Fig. 9).

The general trend is clearly observed in the data from the 0.8 mm and 0.6 mm Nozzle diameter although the data from the 0.4 mm nozzle diameter shows that the specimen with Triangular pattern performed better than the Square pattern. This may be due to unseen errors during the printing or testing phase of the experiment.

Based on the Main Effects Plots in Figs. 6 and 7, it can be hypothesized that testing samples on strain rate of 5 mm/min for tensile tests produces much better results as specimens seem to resist the deformation. Although there seems to be no noticeable pattern between the properties of the 3D printed specimen and the strain rates the specimen were tested according to, the strain rate of 2 mm/min produced the weakest results while the 1 mm/min rate displayed average results.

4. Conclusion

The mechanical properties of 3D printed cellular geometries through different input parameters tested in tension were studied in this paper. Dog bone tensile specimens were modeled through

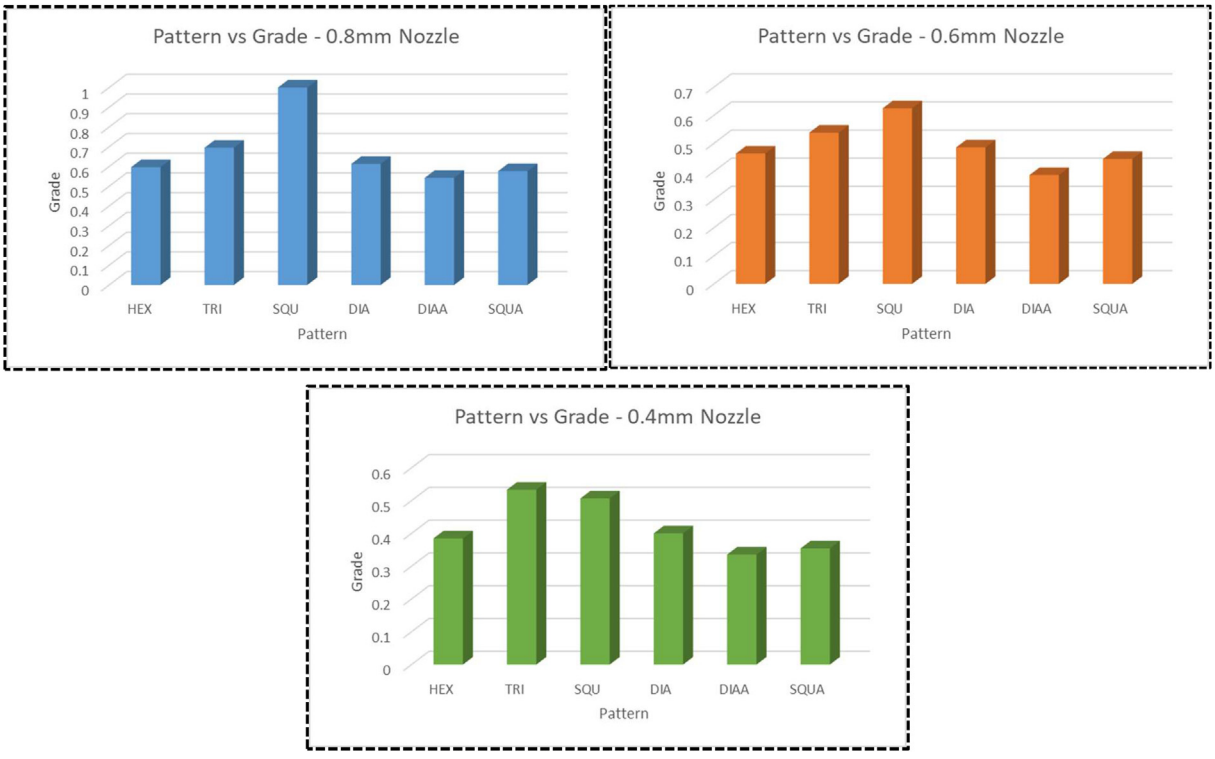

Fig. 9. Comparison of Patterns and their Grade for three nozzle diameters.

CURA software and was printed using a TOBECA 3D printer. Following conclusion have been reported out of the current work.

1. In the light of literature and as per the best knowledge of authors, the current combination of mixed input (printing and testing) parameters with the detailed output responses rarely exists in the literature. It is worth mentioning that Nozzle dia as a parameter is less studied in the literature majority of the work is on layer height, build orientation and print speed. The response data was analyzed for the optimal conditions using grey relational analysis (GRA). This combination of input-out data, and GRA is very rarely found in the existing literature.
2. Six different geometric patterns printed using three different nozzle diameters were studied. Tensile tests were done on the specimens at different three strain rates determined using the Taguchi Model. Through the Minitab 19 software, the optimum pattern, nozzle diameter and strain rates were determined and analyzed. The square geometric pattern demonstrated the best tensile and energy absorption properties.
3. The diamond angle geometric pattern showed relatively poor performance in regard to mechanical properties. Specimens printed with a nozzle diameter of 0.8 mm showed optimized tensile properties when compared to specimens printed with nozzle diameter of 0.4 mm and 0.6 mm.
4. The input parameter that affected the properties the most was the nozzle diameter (48.99%), followed by geometric patterns (40.78%) and strain rate (3.2%). Nozzle diameter has a controlling influence on the mechanical properties of 3D printed samples as it governs the inter layer fusion between the printed material.
5. Through this study, it is observed that the square pattern printed with a nozzle diameter of 0.8 mm and tested at a strain rate of 5 mm/min was the most optimized combination for lightweight applications.

Declaration of competing interest

We wish to confirm that there are no known conflicts of interest associated with this publication and there has been no significant financial support for this work that could have influenced its outcome.

References

[1] A.C. De Leon, Q. Chen, N.B. Palaganas, J.O. Palaganas, J. Manapat, R.C. Advincula, High performance polymer nanocomposites for additive manufacturing applications, React. Funct. Polym. 103 (2016), https://doi.org/10.1016/j.reactfunctpolym.2016.04.010.
[2] H. Wu, W.P. Fahy, S. Kim, H. Kim, N. Zhao, L. Pilato, A. Kafi, S. Bateman, J.H. Koo, Recent developments in polymers/polymer nanocomposites for additive manufacturing, Prog. Mater. Sci. 111 (2020), https://doi.org/10.1016/j.pmatsci.2020.100638.
[3] K. Hibbert, G. Warner, C. Brown, O. Ajide, G. Owolabi, A. Azimi, The effects of build parameters and strain rate on the mechanical properties of FDM 3D-printed acrylonitrile butadiene styrene, Open J. Org. Polym. Mater. 9 (1) (2019) 1–27, https://doi.org/10.4236/ojopm.2019.91001.
[4] Q. Ma, M.R.M. Rejab, A.P. Kumar, H. Fu, N.M. Kumar, J. Tang, Effect of infill pattern, density and material type of 3D printed cubic structure under quasi-static loading, Proc. Inst. Mech. Eng. C J. Mech. Eng. Sci. (2020), https://doi.org/10.1177/0954406220971667.
[5] R. Goutham, T.R. Veena, Babagowda, K.R.S. Prasad, Study on mechanical properties of recycled Acrylonitrile Butadiene Styrene (ABS) blended with virgin Acrylonitrile Butadiene Styrene (ABS) using Taguchi method, Mater. Today Proc. 5 (11) (2018), https://doi.org/10.1016/j.matpr.2018.10.282.
[6] S. Bhandari, R. Lopez-Anido, Finite element analysis of thermoplastic polymer extrusion 3D printed material for mechanical property prediction, Addit. Manuf. 22 (2018), https://doi.org/10.1016/j.addma.2018.05.009.
[7] K.G.J. Christiyan, U. Chandrasekhar, K. Venkateswarlu, A study on the influence of process parameters on the Mechanical Properties of 3D printed ABS composite, IOP Conf. Ser. Mater. Sci. Eng. 114 (1) (2016), https://doi.org/10.1088/1757-899X/114/1/012109.
[8] M. Dawoud, I. Taha, S.J. Ebeid, Mechanical behaviour of ABS: an experimental study using FDM and injection moulding techniques, J. Manuf. Process. 21 (2016), https://doi.org/10.1016/j.jmapro.2015.11.002.
[9] M. Srivastava, S. Maheshwari, T. Kundra, S. Rathee, Multi-response optimization of fused deposition modelling process parameters of ABS using response surface methodology (RSM)-based desirability analysis, Mater. Today Proc. 4 (2) (2017), https://doi.org/10.1016/j.matpr.2017.02.043.
[10] C.A. Griffiths, J. Howarth, G.D.A. Rowbotham, A. Rees, Effect of build parameters on processing efficiency and material performance in fused deposition modelling, Procedia CIRP 49 (2016), https://doi.org/10.1016/j.procir.2015.07.024.
[11] A.R. Torrado, C.M. Shemelya, J.D. English, Y. Lin, R.B. Wicker, D.A. Roberson, Characterizing the effect of additives to ABS on the mechanical property anisotropy of specimens fabricated by material extrusion 3D printing, Addit. Manuf. 6 (2015), https://doi.org/10.1016/j.addma.2015.02.001.
[12] F.S. Senatov, K.V. Niaza, M.Y. Zadorozhnyy, A.V. Maksimkin, S.D. Kaloshkin, Y.Z. Estrin, Mechanical properties and shape memory effect of 3D-printed PLA-based porous scaffolds, J. Mech. Behav. Biomed. Mater. 57 (2016), https://doi.org/10.1016/j.jmbbm.2015.11.036.
[13] J. Fernandes, A.M. Deus, L. Reis, M.F. Vaz, M. Leite, Study of the influence of 3D printing parameters on the mechanical properties of PLA, in: Proceedings of the International Conference on Progress in Additive Manufacturing, 2018-May, 2018, https://doi.org/10.25341/D4988C.
[14] C. Lubombo, M.A. Huneault, Effect of infill patterns on the mechanical performance of lightweight 3D-printed cellular PLA parts, Mater. Today Commun. 17 (2018) 214–228, https://doi.org/10.1016/j.mtcomm.2018.09.017.
[15] M. Kucewicz, P. Baranowski, J. Małachowski, A. Popławski, P. Płatek, Modelling, and characterization of 3D printed cellular structures, Mater. Des. 142 (2018) 177–189, https://doi.org/10.1016/j.matdes.2018.01.028.
[16] M. Kucewicz, P. Baranowski, M. Stankiewicz, M. Konarzewski, P. Płatek, J. Małachowski, Modelling and testing of 3D printed cellular structures under quasi-static and dynamic conditions, Thin-Walled Struct. 145 (2019), https://doi.org/10.1016/j.tws.2019.106385.
[17] S. Kannan, R. Vezhavendhan, S. Kishore, K.V. Kanumuru, Investigating the effect of orientation, infill density with Triple raster pattern on the tensile properties for 3D Printed samples, IOP SciNotes 1 (2) (2020), https://doi.org/10.1088/2633-1357/abb290.
[18] M. Bodaghi, A.R. Damanpack, G.F. Hu, W.H. Liao, Large deformations of soft metamaterials fabricated by 3D printing, Mater. Des. 131 (2017), https://doi.org/10.1016/j.matdes.2017.06.002.
[19] M. Moradi, A. Aminzadeh, D. Rahmatabadi, A. Hakimi, Experimental investigation on mechanical characterization of 3D printed PLA produced by fused deposition modeling (FDM), Mater. Res. Express 8 (3) (2021), https://doi.org/10.1088/2053-1591/abe8f3.
[20] F.N. Mullaveettil, R. Dauksevicius, Y. Wakjira, Strength and elastic properties of 3D printed PVDF-based parts for lightweight biomedical applications, J. Mech. Behav. Biomed. Mater. 120 (2021), https://doi.org/10.1016/j.jmbbm.2021.104603.
[21] M. Moradi, S. Meiabadi, A. Kaplan, 3D printed parts with honeycomb internal pattern by fused deposition modelling; experimental characterization and production optimization, Met. Mater. Int. 25 (5) (2019) 1312–1325, https://doi.org/10.1007/s12540-019-00272-9.
[22] C.K. Yeoh, C.S. Cheah, R. Pushpanathan, C.C. Song, M.A. Tan, P.L. Teh, Effect of infill pattern on mechanical properties of 3D printed PLA and cPLA, IOP Conf. Ser. Mater. Sci. Eng. 957 (1) (2020), https://doi.org/10.1088/1757-899X/957/1/012064.
[23] S.F. Khan, H. Zakaria, Y.L. Chong, M.A.M. Saad, K. Basaruddin, Effect of infill on tensile and flexural strength of 3D printed PLA parts, IOP Conf. Ser. Mater. Sci. Eng. 429 (1) (2018), https://doi.org/10.1088/1757-899X/429/1/012101.
[24] B. Akhoundi, A.H. Behravesh, Effect of filling pattern on the tensile and flexural mechanical properties of FDM 3D printed products, Exp. Mech. 59 (6) (2019), https://doi.org/10.1007/s11340-018-00467-y.
[25] M.N.F. Saniman, M.H.M. Hashim, K.A. Mohammad, K.A.A. Wahid, W.M.W. Muhamad, N.H.N. Mohamed, Tensile characteristics of low density infill patterns for mass reduction of 3D printed polylactic parts, Int. J. Automot. Mech. Eng. 17 (2) (2020), https://doi.org/10.15282/ijame.17.2.2020.11.0592.
[26] V. Cabreira, R.M.C. Santana, Effect of infill pattern in fused filament fabrication (FFF) 3D printing on materials performance, Rev. Mater. 25 (3) (2020), https://doi.org/10.1590/s1517-707620200003.1126.
[27] I. Buj-Corral, A. Bagheri, A. Domínguez-Fernández, R. Casado-López, Influence of infill and nozzle diameter on porosity of FDM printed parts with rectilinear grid pattern, Procedia Manuf. 41 (2019), https://doi.org/10.1016/j.promfg.2019.09.011.
[28] M.S. Hussin, S. Hamat, S.A.S. Ali, M.A.A. Fozi, Y.A. Rahim, M.S.I.M. Dawi, M. Darsin, Experimental and finite element modeling of partial infill patterns for thermoplastic polymer extrusion 3D printed material using elasto-plastic method, AIP Conf. Proc. 2278 (2020), https://doi.org/10.1063/5.0014978.

[29] M.P.G. Chandrashekarappa, G.R. Chate, V. Parashivamurthy, B.S. Kumar, M.A.N. Bandukwala, A. Kaisar, K. Giasin, D.Y. Pimenov, S. Wojciechowski, Analysis and optimization of dimensional accuracy and porosity of high impact polystyrene material printed by FDM process: PSO, JAYA, Rao, and bald eagle search algorithms, Materials 14 (23) (2021) 1–20, https://doi.org/10.3390/ma14237479.

[30] J.S. Chohan, R. Kumar, T.C.B. Singh, S. Singh, S. Sharma, J. Singh, M. Mia, D.Y. Pimenov, S. Chattopadhyaya, S.P. Dwivedi, W. Kapłonek, Taguchi s/n and topsis based optimization of fused deposition modelling and vapor finishing process for manufacturing of ABS plastic parts, Materials 13 (22) (2020) 1–15, https://doi.org/10.3390/ma13225176.

[31] J.S. Chohan, N. Mittal, R. Kumar, S. Singh, S. Sharma, J. Singh, K.V. Rao, M. Mia, D.Y. Pimenov, S.P. Dwivedi, Mechanical strength enhancement of 3d printed acrylonitrile butadiene styrene polymer components using neural network optimization algorithm, Polymers 12 (10) (2020) 1–18, https://doi.org/10.3390/polym12102250.

[32] M.R. Khosravani, T. Reinicke, Effects of raster layup and printing speed on strength of 3D-printed structural components, Procedia Struct. Integr. 28 (2020) 720–725, https://doi.org/10.1016/j.prostr.2020.10.083.

[33] S. Abdallah, S. Ali, S. Pervaiz, Performance optimization of 3D printed polyamide 12 via MultiJet fusion: a Taguchi grey relational analysis (TGRA), Int. J. Lightweight Mater. Manuf. (2022), https://doi.org/10.1016/j.ijlmm.2022.05.004.